https://doi.org/10.1093/plphys/kiac561 PLANT PHYSIOLOGY 2023: 191: 1186–1198

Plant Physiology®

Research Article

Single chloroplast *in folio* imaging sheds light on photosystem energy redistribution during state transitions

Dana Verhoeven [1], **Herbert van Amerongen** [1,2] **and Emilie Wientjes** [1,*]

1 Laboratory of Biophysics, Wageningen University, 6700 ET Wageningen, The Netherlands
2 MicroSpectroscopy Research Facility, Wageningen University, 6700 ET Wageningen, The Netherlands

*Author for correspondence: emilie.wientjes@wur.nl

E.W. and D.V. designed the research, performed the research, analyzed the data, and wrote the paper. H.v.A. provided useful feedback which helped to improve the manuscript.
The author responsible for distribution of materials integral to the findings presented in this article in accordance with the policy described in the Instructions for Authors (https://academic.oup.com/plphys/pages/General-Instructions) is Emilie Wientjes (emilie.wientjes@wur.nl).

Abstract

Oxygenic photosynthesis is driven by light absorption in photosystem I (PSI) and photosystem II (PSII). A balanced excitation pressure between PSI and PSII is required for optimal photosynthetic efficiency. State transitions serve to keep this balance. If PSII is overexcited in plants and green algae, a mobile pool of light-harvesting complex II (LHCII) associates with PSI, increasing its absorption cross-section and restoring the excitation balance. This is called state 2. Upon PSI overexcitation, this LHCII pool moves to PSII, leading to state 1. Whether the association/dissociation of LHCII with the photosystems occurs between thylakoid grana and thylakoid stroma lamellae during state transitions or within the same thylakoid region remains unclear. Furthermore, although state transitions are thought to be accompanied by changes in thylakoid macro-organization, this has never been observed directly in functional leaves. In this work, we used confocal fluorescence lifetime imaging to quantify state transitions in single Arabidopsis (*Arabidopsis thaliana*) chloroplasts *in folio* with sub-micrometer spatial resolution. The change in excitation-energy distribution between PSI and PSII was investigated at a range of excitation wavelengths between 475 and 665 nm. For all excitation wavelengths, the PSI/(PSI + PSII) excitation ratio was higher in state 2 than in state 1. We next imaged the local PSI/(PSI + PSII) excitation ratio for single chloroplasts in both states. The data indicated that LHCII indeed migrates between the grana and stroma lamellae during state transitions. Finally, fluorescence intensity images revealed that thylakoid macro-organization is largely unaffected by state transitions. This single chloroplast *in folio* imaging method will help in understanding how plants adjust their photosynthetic machinery to ever-changing light conditions.

Introduction

Light absorbed by photosystems drives photosynthesis. In oxygenic photosynthesis, photosystem I (PSI) and photosystem II (PSII) work in series. For optimal photosynthetic efficiency, the excitation rates of PSI and PSII should be balanced, even though the absorption spectra of PSI and PSII differ (Pfannschmidt, 2005; Walters, 2005; Taylor et al., 2019). PSI shows more absorption at wavelengths above 680 nm, and around 520 and 420–440 nm, while PSII absorbs

Received June 9, 2022. Accepted November 4, 2022. Advance access publication December 8, 2022

stronger in the 470–500 nm interval, around 560 nm, and around 650–660 nm (Hogewoning et al., 2012; Johnson and Wientjes, 2020; Mattila et al., 2020). Natural variations in the wavelength and intensity of irradiance, for example sun and shade alternation, continuously alter the excitation distribution between the photosystems. State transitions are the acclimation response of the photosynthetic apparatus which is able to rebalance the excitation distribution between the photosystems in about 10 minutes. The antenna sizes of PSI and PSII are adjusted by the association/dissociation of light-harvesting complex II (LHCII) with either PSI or PSII (Allen, 1992; Rochaix, 2014; Goldschmidt-Clermont and Bassi, 2015). State transitions are essential processes, because they enhance plant fitness and were shown to increase CO_2 assimilation in land plants (Lunde et al., 2000; Bellafiore et al., 2005; Frenkel et al., 2007; Tikkanen et al., 2010; Taylor et al., 2019).

State transitions are controlled by the oxidation state of the plastoquinone (PQ) pool, sensed at the Q_0 site of the cytochrome b_6f complex, and regulated by phosphorylation and dephosphorylation of LHCII (Vener et al., 1997; Zito et al., 1999). When PSI is overexcited and the PQ-pool is oxidized, most LHCII is connected to PSII, a condition named state 1. Overexcitation of PSII leads to a reduction of the PQ-pool. Upon over-reduction of the PQ-pool, state 2 is induced: the serine/threonine protein kinase 7 (STN7) is activated which phosphorylates LHCII (Bellafiore et al., 2005). After its phosphorylation, a mobile pool of LHCII antenna dissociates from PSII and connects to PSI, as such decreasing PSII's absorption cross-section and increasing that of PSI. State 1 and state 2 are the two extreme states often induced in experiments; however, under physiological conditions, the thylakoid is usually in an intermediate instead of one of the extremes (Goldschmidt-Clermont and Bassi, 2015).

It is well-known that LHCII binds PSI at the PSI-H, -L, and -O subunits of the PSI core (Kouril et al., 2005; Galka et al., 2012; Pan et al., 2018). In addition, recent work suggests that additional LHCII complexes can transfer energy to PSI, most likely via LHCI (Benson et al., 2015; Bressan et al., 2018; Bos et al., 2019; Schiphorst et al., 2021). Upon dephosphorylation by the protein phosphatase TAP38/PPH1 (Protein phosphatase 1), LHCII dissociates from PSI and associates with PSII (state 1). This phosphatase is assumed to be constitutively active (Pribil et al., 2010; Shapiguzov et al., 2010), meaning that the system returns to State 1 in absence of STN7 activity. Although we generally understand how state transitions are induced, the resulting movement of LHCII and possibly photosystems in the thylakoid membrane is still debated.

A striking feature of the thylakoid membrane is its complex 3D structure, formed from a continuous membrane that encloses a single interior aqueous phase. Stacked cylindrical grana membranes are connected to unstacked stroma lamellae membranes, which are wrapped around the grana (Paolillo, 1970; Bussi et al., 2019). The membranes that connect the grana and stroma lamellae are called slit junctions or grana margins (Mustardy et al., 2008; Rantala et al., 2020). While the majority of PSII is located in the grana stacks, PSI and ATP (adenosine triphosphate) synthase are mostly found in the stroma lamellae (Goodenough and Staehelin, 1971; Andersson and Anderson, 1980; Dekker and Boekema, 2005). Considering the spatial separation of PSI and PSII, phosphorylated LHCII is thought to migrate between PSII in the grana stacks and PSI in the stroma lamellae (Kyle et al., 1983; Larsson et al., 1983, 1987; Bassi et al., 1988). However, it has also been suggested that PSII-LHCII-PSI megacomplexes are formed in the grana margins after LHCII phosphorylation (Tikkanen et al., 2008; Grieco et al., 2015; Suorsa et al., 2015).

The thylakoid macro-organization is thought to dynamically respond to state transitions, following observations obtained with electron microscopy on fixed materials and (structured illumination) microscopy on isolated chloroplasts (Rozak et al., 2002; Chuartzman et al., 2008; Anderson et al., 2012; Pietrzykowska et al., 2014; Iwai et al., 2018; Wood et al., 2018, 2019). Upon the transition to state 2, the number of grana stacks per chloroplast has been reported to increase, while the grana diameter and the number of membranes per stack decreased. Alternatively, it has been suggested that the whole grana organization would disappear (Chuartzman et al., 2008). It is at present unclear how the complex 3D thylakoid architecture can be reconciled with such a high level of plasticity (Johnson and Wientjes, 2020).

The relative PSI and PSII absorbance is a key factor for linear electron transport. Several studies have investigated how much light is absorbed by each photosystem. For spinach (*Spinacia oleracea*) grown under white light conditions, this led to estimated PSI/PSII chlorophyll ratios varying between 0.54 and 1.4. This large spread is most probably partially caused by the indirect measuring techniques used, e.g. gel electrophoresis (Melis et al., 1987) or membrane fractionation (Albertsson, 1995) combined with optical measurements and electron spin resonance (Danielsson et al., 2004). More recently, action spectra of PSI and PSII were resolved *in folio*, which were used to calculate the relative PSI and PSII excitation fraction (Laisk et al., 2014). Confocal microscopy has been used to study the change in the PSI/PSII excitation ratio during state transitions in chloroplasts of protoplasts based on the difference in PSI and PSII emission spectra (Kim et al., 2015). Although changes can be observed with this method, they do not directly reflect the PSI/PSII excitation ratios as the fluorescence quantum yield of PSII is variable and considerably higher than that of PSI. At present, it is not known how the PSI/PSII excitation ratio is affected by state transitions.

Confocal microscopy allows for monitoring the dynamic process of state transitions under nearly physiological conditions, while the spatial resolution in the *x-y* plane is large enough to distinguish grana from other regions of the thylakoid

membrane. Also, the same chloroplast can be imaged in state 1 and state 2, which is impossible with experiments on fixed material. Indeed, single-cell state transitions measurements have recently been demonstrated with advanced fluorescence microscopy methods for algae and cyanobacteria (Bhatti et al., 2021; Zhang et al., 2021).

Here, we use confocal fluorescence lifetime imaging (FLIM) to visualize the grana organization and the energy distribution between PSI and PSII (Wientjes et al., 2017) during state transitions in Arabidopsis (*Arabidopsis thaliana*). With FLIM, a distinction between emission from PSI and PSII is made based on the fluorescence decay kinetics. The fluorescence lifetime of PSI is ≤100 ps for open and closed reaction centers, while the lifetime of PSII with closed reactions centers is about 1–2 ns. FLIM has previously been used to investigate state transitions in the alga *Chlamydomonas reinhardtii* (Iwai et al., 2010). In this work, the energy distribution between PSI and PSII was measured in the grana and stroma lamellae of Arabidopsis in state 1 and state 2 by *in folio* FLIM. Concomitantly, the effect of state transitions on the grana macro-organization was investigated.

Results

Redistributing the energy between PSI and PSII

In this work, confocal fluorescence lifetime imaging (FLIM) is used to investigate state transitions *in folio*. LEDs emitting in the far-red ($\lambda_{max} = 706$ nm) were used to bring the leaves to state 1, while blue LEDs ($\lambda_{max} = 467$ nm) were used to induce state 2, as done before (Bos et al., 2019). Figure 1 shows the LED spectra, the PSI (Wientjes et al., 2011) and PSII (Caffarri et al., 2009) absorption spectra, and the PSI/(PSI + PSII) absorption ratio, demonstrating that the blue light indeed overexcites PSII, while the far-red light overexcites PSI.

The PSI/(PSI + PSII) excitation ratio will be assessed based on the fluorescence decay kinetics of the chlorophyll emission. State 1 and state 2 Arabidopsis leaves will be compared for a range of excitation wavelengths. Based on the different fluorescence lifetimes of PSI (≤ 100 ps for open and closed reaction centers) (Croce et al., 2000; Slavov et al., 2008; Wientjes and Croce, 2012) and PSII (1–2 ns for closed reaction centers) (Roelofs et al., 1992; Matsubara and Chow, 2004; Wientjes et al., 2017), the relative contribution of each photosystem can be quantified. The PSI/(PSI + PSII) excitation fraction can be calculated based on the fraction of ≤100 ps PSI decay and the contribution of PSI and PSII emission at the detection wavelengths, see "Materials and Methods" and Wientjes *et al.* (2017). For this method, it is essential that the PSII reaction centers are closed, such that their lifetime is in the nanosecond range and can be easily separated from the faster PSI decay. This means that the laser power used to excite the sample in the microscope should be high enough to close the reaction centers. However, the laser intensity should not be too high, since that can induce nonphotochemical quenching, damage the photosystems, and/or lead to singlet-triplet annihilations, thereby shortening the fluorescence lifetime (Barzda et al., 2001). For 488 nm light, several laser intensities were tested, and an intensity of 0.12 µW was found to fulfill the requirements (Supplemental Figure 1). This laser intensity was verified to be suitable for other excitation wavelengths as well and used for further experiments.

A balanced PSI verus PSII excitation pressure is essential for optimal linear electron transport. How state transitions affect the wavelength-dependent PSI versus PSII excitation ratio has not been reported yet. Using the FLIM based method, the PSI/(PSI + PSII) excitation ratio was measured for eight excitation wavelengths within the spectral region of photosynthetically active radiation. The far-red (state 1) and blue (state 2) lights were used to induce state 1 or state 2 in wild-type (WT) plants. The same light conditions were used on STN7 plants, locked in state 1, as negative control. FLIM images were recorded after excitation with the following wavelengths: 475, 488, 515, 561, 594, 633, 650 and 665 nm. Next, the PSI/(PSI + PSII) excitation ratio was calculated (Figure 2). For WT plants, the energy distribution between PSI and PSII is different for state 1 and state 2 at all measured excitation wavelengths (*P* value of Student's *t* test <0.001). Instead, for STN7 plants, the PSI/(PSI + PSII) values of both light conditions overlap. For WT plants, the difference in excitation-energy distribution between the photosystems in state 1 and 2 is similar for the different excitation wavelengths. Excitation with 488 nm laser light was used in the following experiments.

State-transitions under the microscope

Next, we aimed to study state-transitions at the level of single chloroplasts. First, we checked if state transitions can be reversibly induced in leaf sections of WT plants, while STN7 plants were used as a negative control. The plants were illuminated with far-red light (state 1 condition), and a leaf section was placed between a microscope slide and a cover glass. Three chloroplasts were imaged with 488 nm excitation light. Then, the sample was illuminated for 30 minutes on the microscope with blue light (state 2 condition), and three other chloroplasts were imaged. Finally, the sample was illuminated for 12 minutes with far-red light after which three chloroplasts were imaged again. For every image, the PSI/(PSI + PSII) excitation ratio was calculated from the fluorescence decay kinetics. The results are shown in Supplemental Figure 2. For WT plants, the PSI/(PSI + PSII) excitation ratio was 0.39 ± 0.01 in state 1, increased to 0.42 ± 0.01 upon transitioning to state 2 and reversed to 0.35 ± 0.00 when going again to state 1 conditions. As expected for STN7, state 1 and state 2 light conditions do not substantially affect the PSI/(PSI + PSII) excitation ratio. This shows that state-transitions were successfully induced in the leaf section under the microscope. Afterwards, we investigated the reversibility when state transitions are induced and a single chloroplast is followed. The chloroplast was imaged in

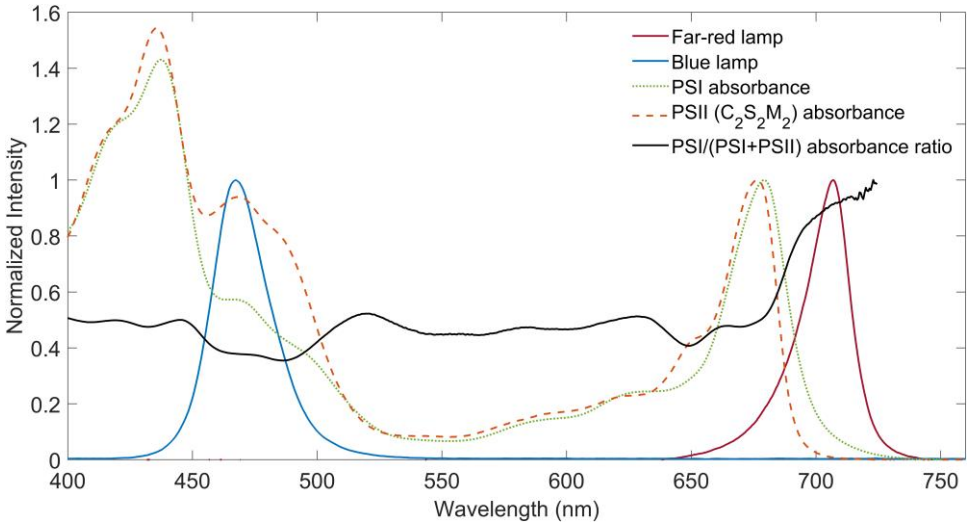

Figure 1 Absorption of photosystems and lamp spectra. Intensity spectra of the far-red ($\lambda_{max} = 705$ nm) and blue lamp ($\lambda_{max} = 467$ nm) used in the experiments to induce state 1 and state 2, respectively, PSI and PSII ($C_2S_2M_2$) absorbance spectra (normalized to their Q_y maximum), and PSI/(PSI + PSII) absorbance ratio spectrum.

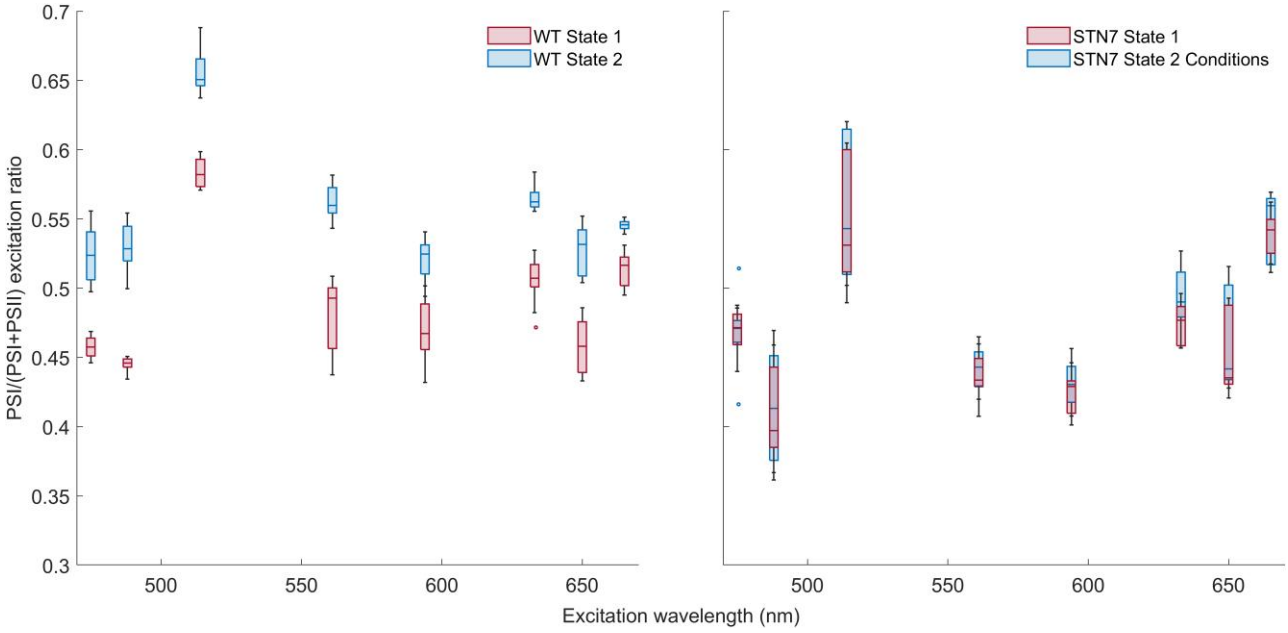

Figure 2 PSI/(PSI + PSII) excitation ratio of WT and STN7 leaves of Arabidopsis measured using FLIM. The leaves were imaged in state 1 and state 2 at various excitation wavelengths. The measurements are displayed in a boxplot. The middle line gives the median of the data. The values inside the box represent 50% of the measured data, and the whiskers together with the box comprise 95% of the measured values; number of chloroplasts imaged per condition is 9. The circles that remain are the outliers. State 1 and state 2 are significantly different in WT at all measured excitation wavelengths with a *P*-value of the Student's *t* test of $P < 0.001$.

state 1, then in state 2 and again in state 1. The results are shown in Supplemental Figure 3. The increased PSI/(PSI + PSII) excitation ratio upon transition to state 2 is reversed when state-1 conditions are applied. These results show that state transitions can be successfully induced under the microscope and that it is possible to follow the changes in a single chloroplast.

Evaluating state transitions at the single chloroplast level

The FLIM-based method allows to assess the PSI/(PSI + PSII) excitation ratio and the overall thylakoid organization *in folio* with sub-micrometer resolution. WT and STN7 leaves were illuminated with far-red, state-1-inducing light and a chloroplast was imaged. Then, while the chloroplast was still in the

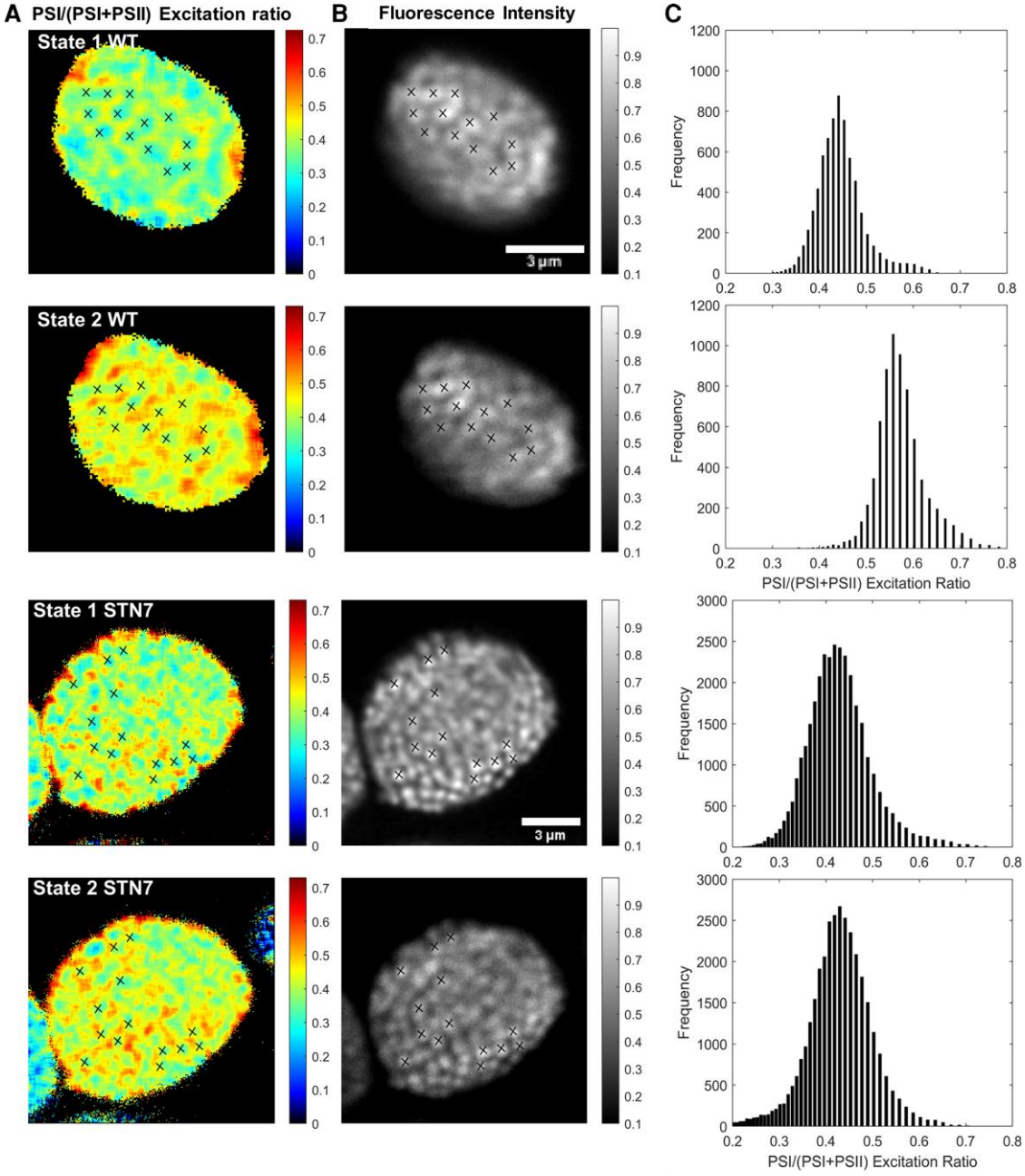

Figure 3 Fluorescence lifetime images of WT and STN7 Arabidopsis plants in state 1 and state 2. A, The PSI/(PSI + PSII) excitation ratio. B, The fluorescence intensity. C, Histogram with the PSI/(PSI + PSII) excitation ratios and their counted pixel frequency are shown. In the rows from top to bottom, state 1 and state 2 from WT and state 1 and state 2 from STN7 are shown. The crosses mark the grana stacks that can be found on the fluorescence intensity image of state 1. The same crosses are displayed on the PSI/(PSI + PSII) excitation ratio images and fluorescence intensity image of state 2. Because of chloroplast movement in between the measurements, the markers had to be rotated 7 degrees for WT, to fit the fluorescence intensity and PSI/(PSI + PSII) excitation ratio images of state 2. To avoid fitting noise, the background fluorescence signal (typically 10% of the maximum fluorescence intensity) was removed.

focus of the microscope objective, the leaf sample was illuminated for 8 minutes with blue light, and the same chloroplast was imaged again (Figure 3).

Figure 3, A and B shows the PSI/(PSI + PSII) excitation ratio (A) and the fluorescence intensity (B) of the same chloroplast in state 1 and state 2 from WT and STN7 plants. The grana stacks show up as bright spots in the fluorescence intensity images, while the stroma lamellae show up as dimly fluorescent areas in between (Gunning and Schwartz, 1999; Kim et al., 2015). As a guide to the eye, a selection of grana

is indicated with cross markings in state 1. The marks are shown at the same position in the PSI/(PSI + PSII) excitation ratio image. As expected, the grana stacks show a lower PSI/(PSI + PSII) excitation ratio, compared with the stroma lamellae membranes located in between, in agreement with the enrichment of PSII in the grana and PSI in the stroma lamellae and with earlier observations (Wientjes et al., 2017). The cross markings are also shown in the state 2 chloroplast. The chloroplasts moved slightly during the 8 minute state-2-inducing illumination period. To correct for the displacement the markings had to be shifted in the *x*, *y* plane and in the case of WT also rotated by 7 degrees. However the position of the cross markings relative to each other is the same as in state 1. From the images of the WT chloroplast (Figure 3 and Supplemental Figure 4 for more examples), it is clear that more energy is transferred to PSI in state 2 than in state 1, both in the stroma lamellae as well as in the grana. This is supported by the PSI/(PSI + PSII) excitation ratio distribution histogram of the pixels (Figure 3C) from the images in Figure 3A, which shows a shift to higher ratios upon state 2 induction. For the WT chloroplast, the average PSI/(PSI + PSII) excitation ratio was 0.45 for state 1 and 0.58 for state 2 ($\lambda_{ex} = 488$ nm). On the other hand, the STN7 chloroplast shows a comparable energy distribution for both states, with an average PSI/(PSI + PSII) excitation ratios of 0.42 for state 1 and 0.42 for state 2 illumination conditions. From these results, it can be concluded that the observed redistribution of excitation energy in the WT chloroplasts is caused by the state 1 to state 2 transition.

The thylakoid macro-organization is largely unaffected by state transitions

To investigate the effect of state transitions on the thylakoid macro-organization, WT chloroplasts were imaged *in folio* in state 1, illuminated for 8 minutes with blue light and next imaged in state 2. The PSI/(PSI + PSII) excitation ratio images show that the state 1 and state 2 were successfully induced (Supplemental Figure 4). Due to chloroplast movement, it was only possible to image the same chloroplast after the 8 minute state-2-inducing light treatment in roughly 30%–40% of the cases. If the chloroplasts move in the imaging plane or in the *z*-direction, it is possible to correct for this and the two states can be compared. However, when the chloroplasts rotate such that a side view instead of a top view is observed, it is impossible to compare the thylakoid organization between the two states. As chloroplast movement in Arabidopsis is a blue light response (Kagawa et al., 2001; Sakai et al., 2001), we also used red ($\lambda_{max} = 650$ nm) light to induce state 2 and used 514 nm excitation for imaging. However, the chloroplasts still moved, and therefore we decided to keep on using blue light to induce state 2. In Figure 4A, the confocal images of four WT chloroplasts in state 1 and state 2 are shown. In Figure 4B, a selection of grana is marked with crosses to facilitate the comparison of the thylakoid organization in the two states. These images have been corrected for rotations and translations that occurred during the illumination period. The original images are reported in Supplemental Figure 4. More examples of chloroplasts brought from state 1 to state 2 with blue or red light, and from state 2 to state 1 with far-red light, are shown in Supplemental Figure 5. The fluorescence images show that the grana locations are very similar in state 1 and state 2. This qualitative result demonstrates that the overall thylakoid macro-organization, e.g. the location of the grana stacks, is not required for state transitions and in fact does not occur as far as we can see.

Discussion

State transitions

Since the 1980s, state transitions in plants have been extensively investigated (Andersson and Anderson, 1980; Larsson et al., 1987; Bassi et al., 1988; Allen, 1992; Rochaix, 2014; Goldschmidt-Clermont and Bassi, 2015). Most studies have been performed at the leaf level or on fixed or isolated chloroplasts. Instead, in vivo studies at the chloroplast level are limited (Kim et al., 2015; Iwai et al., 2018) and absent at the single thylakoid level. As such, conclusions on changes in the thylakoid macro-organizations are based on ensemble averages and have never been observed directly. In this study, several aspects of the state-transition mechanism are investigated. First, we use a FLIM-based imaging method (Wientjes et al., 2017) for *in folio* quantification of the wavelength dependent photosystem excitation energy distribution in state 1 and state 2. Next, we used the same method to investigate changes in the photosystem excitation-energy distribution at the sub-micrometer level in a single chloroplast. Finally, we investigated the effect of state transitions on the thylakoid macro-organization.

How do state transitions change the photosystem energy distribution?

The wavelength dependence of the excitation balance between PSI and PSII has been studied before (Hogewoning et al., 2012; Laisk et al., 2014). However, its dependence on state transitions has not been reported yet. Here, we obtained the energy distribution between PSI and PSII in state 1 and state 2 in Arabidopsis for a range of excitation wavelengths. Next to WT plants, STN7-deficient (STN7) plants, locked in state 1, were investigated. For WT state 1 (and STN7) plants, PSII was strongly overexcited with 475, 488, 560, 590, and 650 nm light, PSI was overexcited with 514 nm light, while about equal PSI:PSII excitation was observed with 633 and 665 nm light. This is in good agreement with the results in (Hogewoning et al., 2012) in which the excitation ratio was calculated based on in vivo measurements on cucumber (*Cucumis sativus*) plants grown under a white light spectrum.

Often state transitions are quantified based on pulsed amplitude modulation chlorophyll fluorescence measurements after excitation with a single excitation wavelength. The

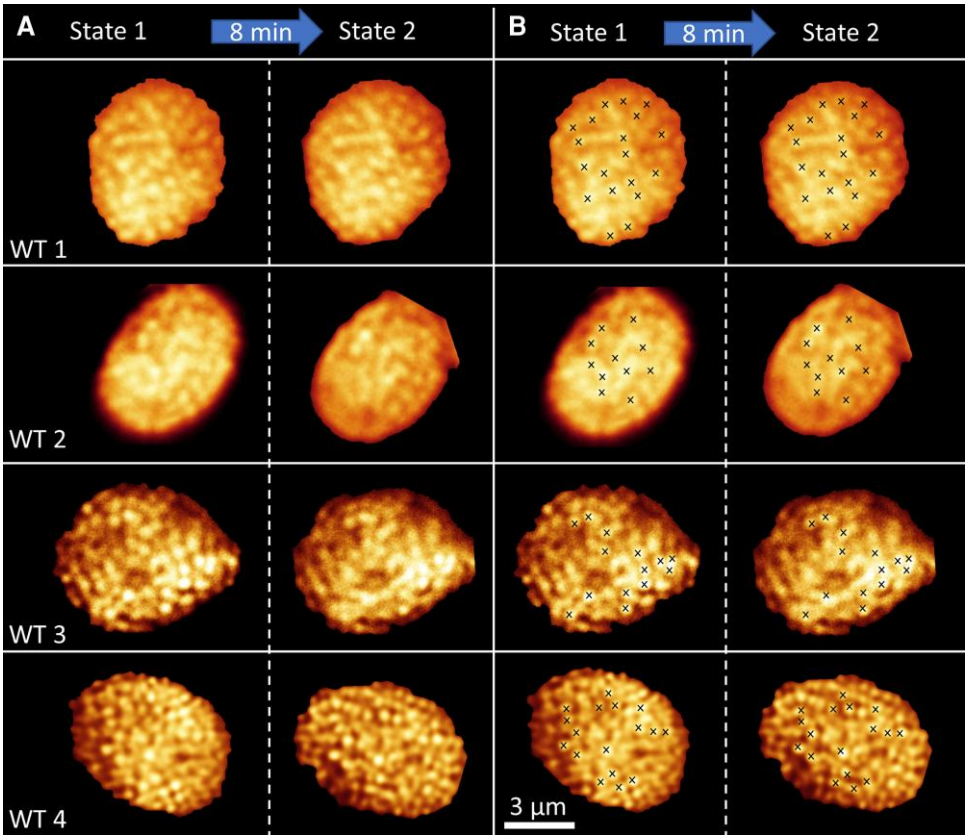

Figure 4 Fluorescence images of WT Arabidopsis chloroplasts in state 1 and state 2. A, Fluorescence intensity image of individual WT chloroplasts imaged first in state 1 and next in state 2. State 2 was induced by 8 minutes illumination with blue light. B, As in (A), but with crosses indicating the bright fluorescence of grana stacks. Individual chloroplast images were digitally extracted for comparison. The scale bar is the same for all images. The contrast and signal to noise ratio of chloroplast WT3 and WT4 was enhanced with HyVolution software of Leica, while chloroplasts WT1 and WT2 are displayed without enhancement. The high similarity between the fluorescence distribution of the same chloroplast in state 1 and state 2 shows that the overall thylakoid macro-organization is largely unaffected by state transitions.

extent of state transitions is given by qT. The qT parameter provides a measure for the change in PSII antenna size based on the maximal fluorescence in state 1 and state 2 (Ruban and Johnson, 2009), $qT = (F_{M'\text{-state-1}} — F_{M'\text{-state-2}})/F_{M'\text{-state 1}}$, with $F_{M'}$ the maximal fluorescence from a light-adapted leaf. The values reported for qT for WT Arabidopsis range from 0.08 to 0.13 (Damkjaer et al., 2009; Wientjes et al., 2013; Benson et al., 2015; Bressan et al., 2018; Sattari Vayghan et al., 2022). To compare the qT values with our measurements, we need to calculate the change in PSII antenna size based on the PSI/(PSI + PSII) excitation ratio. We take the 633 nm excitation data as an example. For state 1, the PSI/(PSI + PSII) excitation ratio was 0.5, increasing to 0.56 for state 2. This equates to a 1:1 PSI:PSII antenna size for state 1 and an 1.12:0.88 PSI:PSII antenna size for state 2, giving a qT value of 0.12. The average qT value of the eight excitation wavelengths was 0.13 ± 0.03. Overall our data agrees reasonably well with the range of qT values reported before.

The qT value only quantifies changes in the PSII antenna size, while state transitions provide a mechanism to adjust the PSI:PSII excitation balance. Our study shows that for the WT Arabidopsis plants grown under white light, PSII is overexcited at most of the tested wavelengths under state 1 conditions, while this shifts to PSI overexcitation under state 2 conditions. This suggests that during evolution Arabidopsis has optimized its antenna system aiming to keep the PSI:PSII excitation energy ratio around unity.

Where do state transitions take place?

At present, at least three models have been proposed that explain the redistribution of excitation energy between PSI and PSII during state transitions. (1) LHCII migrates between the stroma lamellae and the grana stacks, to associate with, respectively, PSI or PSII (Kyle et al., 1983; Larsson et al., 1983, 1987; Bassi et al., 1988). (2) In state 2 PSII, LHCII and PSI migrate to the grana margins and form PSII-LHCII-PSI megacomplexes that increase energy transfer to PSI at the cost of PSII (Tikkanen et al., 2008; Jarvi et al., 2011; Mekala et al., 2015). (3) PSI, LHCII, and PSII are energetically connected in the grana margins in both states; however, LHCII phosphorylation in state 2 enhances the interaction required for efficient energy transfer to PSI (Tikkanen et al., 2008; Grieco et al., 2015).

Here, we present a confocal microscopy–based method to image the state-transition induced change of the

PSI/(PSI + PSII) excitation ratio and thylakoid organization in a single chloroplast within a leaf. This noninvasive method allows for near-native measurement conditions. The lateral (*x*, *y* plane) resolution of confocal microscopy is ≤220 nm, while the radial (*z*-direction) resolution is ≤600 nm. The grana disks have a width ranging from 300 to 600 nm and are typically composed of 2–15 membrane stacks with a repeat distance of ≤20 nm, adding up to a height of 40–300 nm (Dekker and Boekema, 2005; Shimoni et al., 2005; Armbruster et al., 2013; Wood et al., 2019; Li et al., 2020; Sattari Vayghan et al., 2022). The stroma lamellae are wrapped around the grana and are separated by 60–100 nm (Shimoni et al., 2005; Bussi et al., 2019). The lateral resolution allows to discriminate between individual grana stacks. However, in the axial *z*-direction, grana and stroma lamellae membranes are not well resolved. As a consequence, the typical measured PSI/(PSI + PSII) excitation ratios ranged from around 0.25 in the grana to 0.55 in the stroma lamellae (Figure 3, Stn7) for 488 nm light. Instead, a value of 0 would be expected in the grana core and close to 1 for the stroma lamellae when both membrane fractions would be fully resolved (Andersson and Anderson, 1980; Wietrzynski et al., 2020). Despite this limitation in resolution, clearly different PSI/(PSI + PSII) excitation ratios are measured for the two membrane fractions and valuable information on changes in the excitation energy distribution can be acquired.

Figure 3 and Supplemental Figure 4 show that, relative to state 1, in state 2, the PSI excitation is enhanced in both the grana and the stroma lamellae. This is in line with model 1. In state 2 LHCII leaves the grana, resulting in relative less PSII excitation and thus relatively more PSI excitation. The LHCII moved to the stroma lamellae to harvest energy for PSI and thus increasing the PSI excitation in this membrane fraction. This is in agreement with previous findings showing an increased number of LHCII complexes in state 2 stroma lamellae membranes (Kyle et al., 1983; Larsson et al., 1983; Staehelin and Arntzen, 1983; Bressan et al., 2018; Schiphorst et al., 2021). For model 2, the migration of PSI, LHCII, and PSII to the grana margins, an increase in relative PSI excitation would be expected for the grana as PSII is leaving, but in contrast to the results, a decrease in PSI excitation would be expected in the stroma lamellae as the PSI concentration is decreasing in this membrane fraction. Model 3 predicts that in state 2 more energy would be transferred to PSI in the grana margins at the cost of energy transfer to PSII in the grana and grana margins, while no changes in the stroma lamellae are expected. Our data indeed shows an increase in energy transfer to PSI in the grana and grana margins (which are not resolved at diffraction limited resolution). However, our data also shows an increase in energy transfer to PSI in the stroma lamellae, which is not in agreement with model 3. In summary, our data is in agreement with the theory that LHCII relocates between the grana and stroma lamellae during state transitions.

What is the effect of state transitions on the thylakoid macro-organization?

Grana stacking depends on a delicate balance between attractive and repulsive forces (Barber et al., 1980; Puthiyaveetil et al., 2017). The phosphorylation of LHCII in state 2 adds negative charge to LHCII and has been proposed to alter the grana organization (Barber, 1982). Based on ensemble measurements it was concluded that the thylakoid organization changes after several minutes up to 2 hours of exposure to light of different colors or intensity (Rozak et al., 2002; Chuartzman et al., 2008; Anderson et al., 2012; Pietrzykowska et al., 2014; Iwai et al., 2018; Wood et al., 2018, 2019). Relative to state 1 conditions, state 2 shows: 35%–40% less membranes per grana stack (Pietrzykowska et al., 2014; Wood et al., 2018, 2019), 10%–30% more grana stacks per chloroplast (Wood et al., 2018; Wood et al., 2019), and an 15%–35% smaller grana diameter (Iwai et al., 2018; Wood et al., 2018, 2019). As the thylakoid membrane is a tightly interconnected system, changes of this order of magnitude would result in a large overall reorganization of the thylakoid macrostructure within a single chloroplast.

Our confocal microscopy images allow to visualize the thylakoid macro-organization in a single chloroplast under state 1 and state 2 conditions, while the FLIM data provides the evidence that the respective state was indeed successfully induced. Visual inspection of the data presented in Figure 3, Figure 4 and Supplemental Figure 5 shows that the grana locations are largely unaffected by the state 1 to state 2 transition. This means that there are no major changes in the number of grana stacks per thylakoid. Furthermore, it can be hypothesized that the number of membranes per grana stack remains the same, as it seems unlikely that this number can change without an overall reorganization of the intertwined 3D thylakoid membrane architecture. However, the lateral resolution of confocal microscopy is too low to visualize this. A super-resolution in vivo imaging method, which can resolve the number of membranes per grana stack, is required to proof or falsify this hypothesis. Changes in the grana diameter cannot be excluded based on these measurements, as the resolution of our *in folio* confocal microscopy experiment does not allow to resolve small changes in the granum diameter. In fact, a small decrease in the granum diameter is expected as the PSII antenna size decreased by about 12% in state 2, which is ascribed to the migration of LHCII from the grana to the stroma lamellae. If 70%–80% of the granum surface is protein and we assume that this is mostly PSII-LHCII, then a simple calculation tells us that in state 2 the area is expected to decrease with $\leq 0.7 \times 0.12 \times 100\% = 8.4\%$ to 91.6% of the state 1 value. The area scales with the diameter squared, and as such, based on the decreased LHCII content, the granum diameter in state 2 is expected to be ≤96% that of state 1. Changes in the grana swelling and the grana stacking interactions might cause additional changes in the grana diameter (Barber et al., 1980; Puthiyaveetil et al., 2017; Li et al., 2020).

What is causing the discrepancy between our data, showing no change in the number of grana stacks per chloroplast between state 1 and state 2, and previous results that showed a larger number of grana stacks in state 2? An important factor might be the illumination time used to induce a state. While the state 1 to state 2 transition is completed in about 8 minutes and the reverse in 12 minutes (Damkjaer et al., 2009), several studies use an illumination time of 1–2 hours (Pietrzykowska et al., 2014; Iwai et al., 2018; Wood et al., 2018). Wood et al. have shown that the change in thylakoid organization occurs on a longer timescale than state transitions (Wood et al., 2019). Taken together, this could indicate that state transitions have been mistakenly associated with an overall change in the thylakoid architecture, while instead slower processes must be responsible for the thylakoid architectural reorganization.

Conclusions

In this work, we visualize the difference in energy distribution between PSI and PSII as a consequence of state transitions in Arabidopsis. We determine how state transitions redistribute the excitation energy between PSI and PSII. Imaging state transitions in single chloroplasts indicates that the molecular mechanism that drives the excitation energy redistribution is the relocation of LHCII between the grana stacks and the stroma lamellae membranes. Our data shows that the grana macro-organization is largely retained during state transitions. The described single chloroplast *in folio* imaging method is a promising addition to the toolbox for elucidating how plants adapt their photosynthetic machinery to cope with everchanging light conditions.

Materials and methods

Plant material

Arabidopsis (*Arabidopsis thaliana*; Columbia ecotype) WT and STN7-deficient (STN7) plants (SALK_073254) (Bellafiore et al., 2005) were grown in a growth chamber (Hettich Benelux, PRC 1200 WL) with photoperiod 8 hours with intensity 125 µmol photons m^{-2} s^{-1} of white LED light, a relative humidity of 60% and temperature of 22°C during the night and 24°C during the day. Plants of 3–4 weeks were used for the experiments.

Confocal FLIM measurements

Microscope slides were prepared with leaves in the imaging buffer: 0.3 M sorbitol, 20 mM tricine (pH 7.7), 5 mM $MgCl_2$, 2.5 mM EDTA, and 10 mM $NaHCO_3$. The measurements were performed on a confocal Leica TCS SP8 system using a pulsed White Light Laser (Leica Microsystems). The laser intensity ranged from 0.07 to 0.24 µW as indicated in the text. A 63 × 1.2 NA water immersion objective was used, the laser repetition rate was 40 MHz and the scan rate was 100 Hz. The fluorescence was recorded by two detectors. Detector 1 (fluorescence wavelengths from 675 to 685 nm) was used in photon-counting mode for the fluorescence intensity images. Detector 2 (fluorescence wavelengths from 710 to 750 nm) was coupled to a time-correlated single photon counting module (Becker & Hickl GmbH, Berlin, Germany), with 32 ps/channel. Each image was recorded for 30 seconds. During the experiments, different excitation wavelengths (λ_{ex}): 475, 48, 514, 561, 594, 633, 650, and 665 nm, were used, all at laser power 0.12 µW. The image size was 9.2 µm × 9.2 µm with 128 × 128 pixels or 256 × 256 pixels. FLIMfit (Imperial College, London) (Warren et al., 2013) was used to fit the fluorescence decay kinetics. A binning of 3 was used, such that for every pixel the surrounding pixels in a 7 × 7 array are combined, thus greatly improving the signal to noise ratio. The instrument response function was recorded with pinacyanol chloride (Exciton) in methanol (Sigma-Aldrich) (van Oort et al., 2008).

Chloroplasts located close to the leave surface were selected for the measurement to minimize reabsorption of the emitted fluorescence. The PSI/(PSI + PSII) absorption ratio was determined from the fitted fluorescence decay data of detector 2 (710 nm—750 nm emission) as described in earlier work (Wientjes et al., 2017). In short, the fluorescence decay was fitted with three lifetimes, according to Equation 1.

$$F(t) = a_1 \times \exp\left(-\frac{t}{\tau_1}\right) + a_2 \times \exp\left(-\frac{t}{\tau_2}\right) + a_3 \times \exp\left(-\frac{t}{\tau_3}\right) \quad (1)$$

In Equation 1, the amplitudes a_1, a_2, and a_3 give the normalized ($a_1 + a_2 + a_3 = 1$) contributions of the fluorescence corresponding to lifetimes τ_1, τ_2, and τ_3. The shortest lifetime (τ_1) of ≤100 ps is ascribed to PSI, while the two other lifetimes (τ_2 and τ_3) are in the ns-range and are ascribed to PSII. The amplitude of the ≤100 ps PSI lifetime (a_1) depends on the fraction of PSI excitation ($f_{PSI} = \frac{PSI_{excitation}}{PSI_{excitation}+PSII_{excitation}}$), the emission spectra of PSI and PSII, the wavelength dependent detector sensitivity, and the detection wavelength range, according to Equation 2.

$$a_1 = \frac{f_{PSI} \times PSI}{f_{PSI} \times PSI + (1 - f_{PSI}) * PSII} \quad (2)$$

With $PSI = \int_{\lambda_{begin}}^{\lambda_{end}} PSI\ emission \times detector\ sensitivity\ d\lambda$ and $PSII = \int_{\lambda_{begin}}^{\lambda_{end}} PSII\ emission \times detector\ sensitivity\ d\lambda$, in which $PSI_{emission}$ and $PSII_{emission}$ refer to the emission spectra of PSI and PSII, normalized to their total area under the spectra, *detector sensitivity* refers to the wavelength dependent sensitivity of the detector and $\lambda_{begin\text{-}end}$ to the range of emission light that is detected. To measure the detector sensitivity, spectra of Atto 594 (Atto-Tec GmbH) dissolved in dimethyl sulfoxide (Sigma-Aldrich) recorded on a

Fluorolog 3.22 spectrofluorimeter (Jobin Yvon-Spex) and on the Leica TCS SP8 were compared. The PSI and PSII emission spectra and the detector sensitivity are reported in Supplemental Figure S6.

Based on Equation 2, it follows that the PSI/(PSI + PSII) excitation ratio (f_{PSI}) is given by Equation 3. In which *PSI* and *PSII* are described above and a_1 is the measured amplitude of the ≤100 ps lifetime.

$$f_{PSI} = \frac{PSII}{\frac{PSI}{a_1} - PSI + PSII} \quad (3)$$

Laser intensity—For the analysis of the fluorescence decay data, it is essential that the PSII fluorescence lifetime is far longer than 100 ps, so it can be easily separated from the quickly decaying ≤100 ps PSI fluorescence lifetime. To achieve this, the reaction centers of PSII should be closed by the laser used in the experiments. However the laser intensity should not activate nonphotochemical quenching, nor lead to annihilation or PSII damage. To select the laser intensity that fulfills these requirements, the fluorescence decay kinetics of a dark-adapted leaf was compared with that of an DCMU infiltrated leaf (50 µM DCMU (3-(3,4-dichlorophenyl)-1,1-dimethylurea, Sigma-Aldrich). DCMU assures that the PSII reaction centers are closed even under very low light conditions. The fluorescence was recorded from 710 to 750 nm after 488 nm excitation. Laser intensities of 0.07 µW, 0.12 µW, 0.17 µW, 0.24 µW, 0.30 µW and then again 0.07 µW were used. The fluorescence decay kinetics was recorded for 10 seconds per measurement. The laser power of 0.07 µW was measured again to verify that no permanent damage had occurred during the measurements with higher laser power.

State transitions

To investigate the effect of state transitions on the wavelength-dependent PSI/(PSI + PSII), excitation energy distribution state transitions were induced on WT plants, and the same illumination conditions were used on STN7 plants that cannot perform state transitions and were permanently in state 1. For a minimum of 30 minutes, three WT and three STN7 plants were acclimated to 78 µmol photons m^{-2} s^{-1} of far-red light (λ_{max} = 706 nm) to induce state 1. The same number of plants was exposed to 50 µmol photons m^{-2} s^{-1} of blue light (λ_{max} = 467 nm) to induce state 2 in WT plants. From WT and STN7, three leaves originating from three different plants per light treatment were measured. Each leaf was imaged using various excitation wavelengths. For all excitation wavelengths, three individual chloroplasts were imaged per leaf.

To assess the reversibility of the state transitions process for leaf sections placed under the microscope, a WT and a STN7 plant were illuminated for 12 minutes with 78 µmol photons m^{-2} s^{-1} of far-red light (state 1 condition). Three chloroplasts were imaged (size of image 9.2 µm × 9.2 µm), and next the leaf sample on the microscope slide was illuminated for 30 minutes with 25 µmol photons m^{-2} s^{-1} of blue light (λ_{max} = 467 nm, state 2 condition), and three chloroplasts were imaged. The blue light was kept on during the measurement. Next, state 1 was induced again with 40 µmol photons m^{-2} s^{-1} of far-red light for 15 minutes, whereafter three other chloroplasts were imaged.

For measurements on the same chloroplast in state 1 and state 2, the WT and STN7 plants were illuminated for 30 minutes with 78 µmol photons m^{-2} s^{-1} of far-red light (state 1 condition). Next, the FLIM image was recorded in one chloroplast at excitation wavelength λ_{ex} = 488 nm. Then, state 2 was induced by illumination with 25 µmol photons m^{-2} s^{-1} of blue light for 8 minutes. Afterwards, another image was recorded upon excitation with 488 nm light. To evaluate the reversibility of the induced state transitions, one chloroplast from a WT plant was imaged a third time after 30 minutes of dark adaptation to induce state 1.

Statistical analysis

For statistical analysis, two-tailed independent sample *t* tests were used.

Accession numbers

Sequence data from this article can be found in the GenBank/EMBL data libraries under accession number AT1G68830 (STN7).

Data availability

The data underpinning this study can be found at doi 10.4121/20473863.

Supplemental data

The following materials are available in the online version of this article.

Supplemental Figure S1. Effect of laser intensity.

Supplemental Figure S2. Photosystem I/(Photosystem I + Photosystem II) (PSI/(PSI + PSII)) excitation ratio of wild type (WT) and STN7 samples brought to state 1, then to state 2 and again back to state 1.

Supplemental Figure S3. Photosystem I/(Photosystem I + Photosystem II) (PSI/(PSI + PSII)) excitation ratio and fluorescence intensity images of the same chloroplast from WT *Arabidopsis* which is first brought to state 1, then to state 2 and again to state 1.

Supplemental Figure S4. Photosystem I/(Photosystem I + Photosystem II) (PSI/(PSI + PSII)) excitation ratio and fluorescence intensity images of WT chloroplasts which are first brought to state 1 and next to state 2.

Supplemental Figure S5. Fluorescence intensity images of WT chloroplasts in state 1 and state 2.

Supplemental Figure S6. Spectra used to calculate the PSI/(PSI + PSII) excitation ratio based on the ∼100 ps amplitude of the thylakoid fluorescence decay kinetics.

Acknowledgments

Jan Willem Borst and Arjen Bader are acknowledged for excellent technical support.

Funding

This research was supported by the nederlandse organisatie voor wetenschappelijk onderzoek (NWO) via a Vidi grant no. VI.Vidi 192.042 to E.W.

Conflict of interest statement. The authors declare no conflict of interest.

References

Albertsson PA (1995) The structure and function of the chloroplast photosynthetic membrane - a model for the domain organization. Photosyn Res **46**(1–2): 141–149

Allen JF (1992) Protein-phosphorylation in regulation of photosynthesis. Biochim Biophys Acta **1098**(3): 275–335

Anderson JM, Horton P, Kim EH, Chow WS (2012) Towards elucidation of dynamic structural changes of plant thylakoid architecture. Philos Trans R Soc Lond B Biol Sci **367**(1608): 3515–3524

Andersson B, Anderson JM (1980) Lateral heterogeneity in the distribution of chlorophyll-protein complexes of the thylakoid membranes of spinach chloroplasts. Biochim Biophys Acta **593**(2): 427–440

Armbruster U, Labs M, Pribil M, Viola S, Xu WT, Scharfenberg M, Hertle AP, Rojahn U, Jensen PE, Rappaport F, et al. (2013) Arabidopsis CURVATURE THYLAKOID1 proteins modify thylakoid architecture by inducing membrane curvature. Plant Cell **25**(7): 2661–2678

Barber J (1982) Influence of surface-charges on thylakoid structure and function. Annu Rev Plant Physiol Plant Mol Biol **33**(1): 261–295

Barber J, Chow WS, Scoufflaire C, Lannoye R (1980) The relationship between thylakoid stacking and salt induced chlorophyll fluorescence changes. Biochim Biophys Acta **591**(1): 92–103

Barzda V, de Grauw CJ, Vroom J, Kleima FJ, van Grondelle R, van Amerongen H, Gerritsen HC (2001) Fluorescence lifetime heterogeneity in aggregates of LHCII revealed by time-resolved microscopy. Biophys J **81**(1): 538–546

Bassi R, Giacometti G, Simpson D (1988) Changes in the organization of stroma membranes induced by in vivo state 1-state 2 transition. BBA **935**(2): 152–165

Bellafiore S, Bameche F, Peltier G, Rochaix JD (2005) State transitions and light adaptation require chloroplast thylakoid protein kinase STN7. Nature **433**(7028): 892–895

Benson SL, Maheswaran P, Ware MA, Hunter CN, Horton P, Jansson S, Ruban AV, Johnson MP (2015) An intact light harvesting complex I antenna system is required for complete state transitions in Arabidopsis. Nat Plants **1**(12): 1–9 (Article number 15176)

Bhatti AF, Kirilovsky D, van Amerongen H, Wientjes E (2021) State transitions and photosystems spatially resolved in individual cells of the cyanobacterium *Synechococcus elongatus*. Plant Physiol **186**(1): 569–580

Bos P, Oosterwijk A, Koehorst R, Bader A, Philippi J, van Amerongen H, Wientjes E (2019) Digitonin-sensitive LHCII enlarges the antenna of photosystem I in stroma lamellae of *Arabidopsis thaliana* after far-red and blue-light treatment. Biochim Biophys Acta Bioenerg **1860**(8): 651–658

Bressan M, Bassi R, Dall'Osto L (2018) Loss of LHCI system affects LHCII re-distribution between thylakoid domains upon state transitions. Photosynth Res **135**(1–3): 251–261

Bussi Y, Shimoni E, Weiner A, Kapon R, Charuvi D, Nevo R, Efrati E, Reich Z (2019) Fundamental helical geometry consolidates the plant photosynthetic membrane. Proc Natl Acad Sci U S A **116**(44): 22366–22375

Caffarri S, Kouril R, Kereiche S, Boekema EJ, Croce R (2009) Functional architecture of higher plant photosystem II supercomplexes. Embo J **28**(19): 3052–3063

Chuartzman SG, Nevo R, Shimoni E, Charuvi D, Kiss V, Ohad I, Brumfeld V, Reich Z (2008) Thylakoid membrane remodeling during state transitions in Arabidopsis. Plant Cell **20**(4): 1029–1039

Croce R, Dorra D, Holzwarth AR, Jennings RC (2000) Fluorescence decay and spectral evolution in intact photosystem I of higher plants. Biochemistry **39**(21): 6341–6348

Damkjaer JT, Kereiche S, Johnson MP, Kovacs L, Kiss AZ, Boekema EJ, Ruban AV, Horton P, Jansson S (2009) The photosystem II light-harvesting protein Lhcb3 affects the macrostructure of photosystem II and the rate of state transitions in Arabidopsis. Plant Cell **21**(10): 3245–3256

Danielsson R, Albertsson PA, Mamedov F, Styring S (2004) Quantification, of photosystem I and II in different parts of the thylakoid membrane from spinach. Biochim Biophys Acta Bioenerg **1608**(1): 53–61

Dekker JP, Boekema EJ (2005) Supramolecular organization of thylakoid membrane proteins in green plants. BBA Bioenerg **1706**(1–2): 12–39

Frenkel M, Bellafiore S, Rochaix JD, Jansson S (2007) Hierarchy amongst photosynthetic acclimation responses for plant fitness. Physiol Plant **129**(2): 455–459

Galka P, Santabarbara S, Khuong TT, Degand H, Morsomme P, Jennings RC, Boekema EJ, Caffarri S (2012) Functional analyses of the plant photosystem I-light-harvesting complex II supercomplex reveal that light-harvesting complex II loosely bound to photosystem II is a very efficient antenna for photosystem I in state II. Plant Cell **24**(7): 2963–2978

Goldschmidt-Clermont M, Bassi R (2015) Sharing light between two photosystems: mechanism of state transitions. Curr Opin Plant Biol **25**: 71–78

Goodenough UW, Staehelin LA (1971) Structural differentiation of stacked and unstacked chloroplast membranes - freeze-etch electron microscopy of wild-type and mutant strains of chlamydomonas. J Cell Biol **48**(3): 594–619

Grieco M, Suorsa M, Jajoo A, Tikkanen M, Aro EM (2015) Light-harvesting II antenna trimers connect energetically the entire photosynthetic machinery - including both photosystems II and I. Biochim Biophys Acta **1847**(6–7): 607–619

Gunning BES, Schwartz OM (1999) Confocal microscopy of thylakoid autofluorescence in relation to origin of grana and phylogeny in the green algae. Aust J Plant Physiol **26**(7): 695–708

Hogewoning SW, Wientjes E, Douwstra P, Trouwborst G, van Ieperen W, Croce R, Harbinson J (2012) Photosynthetic quantum yield dynamics: from photosystems to leaves. Plant Cell **24**(5): 1921–1935

Iwai M, Roth MS, Niyogi KK (2018) Subdiffraction-resolution live-cell imaging for visualizing thylakoid membranes. Plant J **96**(1): 233–243

Iwai M, Yokono M, Inada N, Minagawa J (2010) Live-cell imaging of photosystem II antenna dissociation during state transitions. Proc Natl Acad Sci U S A **107**(5): 2337–2342

Jarvi S, Suorsa M, Paakkarinen V, Aro EM (2011) Optimized native gel systems for separation of thylakoid protein complexes: novel super- and mega-complexes. Biochem J **439**(2): 207–214

Johnson MP, Wientjes E (2020) The relevance of dynamic thylakoid organisation to photosynthetic regulation. Biochim Biophys Acta Bioenerg **1861**(4): 148039

Kagawa T, Sakai T, Suetsugu N, Oikawa K, Ishiguro S, Kato T, Tabata S, Okada K, Wada M (2001) Arabidopsis NPL1: a phototropin homolog controlling the chloroplast high-light avoidance response. Science **291**(5511): 2138–2141

Kim E, Ahn TK, Kumazaki S (2015) Changes in antenna sizes of photosystems during state transitions in granal and stroma-exposed

thylakoid membrane of intact chloroplasts in Arabidopsis mesophyll protoplasts. Plant Cell Physiol **56**(4): 759–768

Kouril R, Arteni AA, Lax J, Yeremenko N, D'Haene S, Rogner M, Matthijs HCP, Dekker JP, Boekema EJ (2005) Structure and functional role of supercomplexes of IsiA and photosystem I in cyanobacterial photosynthesis. FEBS Lett **579**(15): 3253–3257

Kyle DJ, Staehelin LA, Arntzen CJ (1983) Lateral mobility of the light-harvesting Complex in chloroplast membranes controls excitation-energy distribution in higher-plants. Arch Biochem Biophys **222**(2): 527–541

Laisk A, Oja V, Eichelmann H, Dall'Osto L (2014) Action spectra of photosystems II and I and quantum yield of photosynthesis in leaves in state 1. Biochim Biophys Acta **1837**(2): 315–325

Larsson UK, Jergil B, Andersson B (1983) Changes in the lateral distribution of the light-harvesting chlorophyll-a/b–protein complex induced by its phosphorylation. Eur J Biochem **136**(1): 25–29

Larsson UK, Sundby C, Andersson B (1987) Characterization of 2 different subpopulations of spinach light-harvesting chlorophyll a/B-protein complex (lhc-ii) - polypeptide composition. Phosphorylation pattern and association with photosystem-II. BBA **894**(1): 59–68

Li M, Mukhopadhyay R, Svoboda V, Oung HMO, Mullendore DL, Kirchhoff H (2020) Measuring the dynamic response of the thylakoid architecture in plant leaves by electron microscopy. Plant Direct **4**(11): e00280

Lunde C, Jensen PE, Haldrup A, Knoetzel J, Scheller HV (2000) The PSI-H subunit of photosystem I is essential for state transitions in plant photosynthesis. Nature **408**(6812): 613–615

Matsubara S, Chow WS (2004) Populations of photoinactivated photosystem II reaction centers characterized by chlorophyll a fluorescence lifetime in vivo. Proc Natl Acad Sci U S A **101**(52): 18234–18239

Mattila H, Khorobrykh S, Hakala-Yatkin M, Havurinne V, Kuusisto I, Antal T, Tyystjarvi T, Tyystjarvi E (2020) Action spectrum of the redox state of the plastoquinone pool defines its function in plant acclimation. Plant J **104**(4): 1088–1104

Melis A, Spangfort M, Andersson B (1987) Light-Absorption and electron-transport balance between photosystem-ii and photosystem-I in spinach-chloroplasts. Photochem Photobiol **45**(1): 129–136

Mekala NR, Suorsa M, Rantala M, Aro EM, Tikkanen M (2015) Plants actively avoid state transitions upon changes in light intensity: role of light-harvesting complex II protein dephosphorylation in high light. Plant Physiol **168**(2): 721–734

Mustardy L, Buttle K, Steinbach G, Garab G (2008) The three-dimensional network of the thylakoid membranes in plants: quasihelical model of the granum-stroma assembly. Plant Cell **20**(10): 2552–2557

Pan XW, Ma J, Su XD, Cao P, Chang WR, Liu ZF, Zhang XZ, Li M (2018) Structure of the maize photosystem I supercomplex with light-harvesting complexes I and II. Science **360**(6393): 1109–1113

Paolillo DJ J (1970) The three-dimensional arrangement of intergranal lamellae in chloroplasts. J Cell Sci **6**(1): 243–253

Pfannschmidt T (2005) Acclimation to varying light qualities: toward the functional relationship of state transitions and adjustment of photosystem stoichiometry. J Phycol **41**(4): 723–725

Pietrzykowska M, Suorsa M, Semchonok DA, Tikkanen M, Boekema EJ, Aro EM, Jansson S (2014) The light-harvesting chlorophyll a/b binding proteins Lhcb1 and Lhcb2 play complementary roles during state transitions in Arabidopsis. Plant Cell **26**(9): 3646–3660

Pribil M, Pesaresi P, Hertle A, Barbato R, Leister D (2010) Role of plastid protein phosphatase TAP38 in LHCII dephosphorylation and thylakoid electron flow. PLoS Biol **8**(1):e1000288

Puthiyaveetil S, van Oort B, Kirchhoff H (2017) Surface charge dynamics in photosynthetic membranes and the structural consequences. Nat Plants **3**(4): 1–9

Rantala M, Rantala S, Aro EM (2020) Composition, phosphorylation and dynamic organization of photosynthetic protein complexes in plant thylakoid membrane. Photochem Photobiol Sci **19**(5): 604–619

Rochaix JD (2014) Regulation and dynamics of the light-harvesting system. Annu Rev Plant Biol **65**(1): 287–309

Roelofs TA, Lee CH, Holzwarth AR (1992) Global target analysis of picosecond chlorophyll fluorescence kinetics from pea chloroplasts: a new approach to the characterization of the primary processes in photosystem II alpha- and beta-units. Biophys J **61**(5): 1147–1163

Rozak PR, Seiser RM, Wacholtz WF, Wise RR (2002) Rapid, reversible alterations in spinach thylakoid appression upon changes in light intensity. Plant Cell Environ **25**(3): 421–429

Ruban AV, Johnson MP (2009) Dynamics of higher plant photosystem cross-section associated with state transitions. Photosyn Res **99**(3): 173–183

Sakai T, Kagawa T, Kasahara M, Swartz TE, Christie JM, Briggs WR, Wada M, Okada K (2001) Arabidopsis nph1 and npl1: blue light receptors that mediate both phototropism and chloroplast relocation. Proc Natl Acad Sci USA **98**(12): 6969–6974

Sattari Vayghan H, Nawrocki WJ, Schiphorst C, Tolleter D, Hu C, Douet V, Glauser G, Finazzi G, Croce R, Wientjes E, et al. (2022) Photosynthetic light harvesting and thylakoid organization in a CRISPR/Cas9 *Arabidopsis thaliana* LHCB1 knockout mutant. Front Plant Sci **13**: 833032

Schiphorst C, Achterberg L, Gomez R, Koehorst R, Bassi R, van Amerongen H, Dall'Osto L, Wientjes E (2021) The role of light-harvesting complex I in excitation-energy transfer from LHCII to photosystem I in Arabidopsis. Plant Physiol **188**(4): 1–12

Shapiguzov A, Ingelsson B, Samol I, Andres C, Kessler F, Rochaix JD, Vener AV, Goldschmidt-Clermont M (2010) The PPH1 phosphatase is specifically involved in LHCII dephosphorylation and state transitions in *Arabidopsis*. Proc Natl Acad Sci U S A **107**(10): 4782–4787

Shimoni E, Rav-Hon O, Ohad I, Brumfeld V, Reich Z (2005) Three-dimensional organization of higher-plant chloroplast thylakoid membranes revealed by electron tomography. Plant Cell **17**(9): 2580–2586

Slavov C, Ballottari M, Morosinotto T, Bassi R, Holzwarth AR (2008) Trap-limited charge separation kinetics in higher plant photosystem I complexes. Biophys J **94**(9): 3601–3612

Staehelin LA, Arntzen CJ (1983) Regulation of chloroplast membrane function: protein phosphorylation changes the spatial organization of membrane components. J Cell Biol **97**(5): 1327–1337

Suorsa M, Rantala M, Mamedov F, Lespinasse M, Trotta A, Grieco M, Vuorio E, Tikkanen M, Jarvi S, Aro EM (2015) Light acclimation involves dynamic re-organization of the pigment-protein megacomplexes in non-appressed thylakoid domains. Plant J **84**(2): 360–373

Taylor CR, van Ieperen W, Harbinson J (2019) Demonstration of a relationship between state transitions and photosynthetic efficiency in a higher plant. Biochem J **476**(21): 3295–3312

Tikkanen M, Grieco M, Kangasjarvi S, Aro EM (2010) Thylakoid protein phosphorylation in higher plant chloroplasts optimizes electron transfer under fluctuating light. Plant Physiol **152**(2): 723–735

Tikkanen M, Nurmi M, Suorsa M, Danielsson R, Mamedov F, Styring S, Aro EM (2008) Phosphorylation-dependent regulation of excitation energy distribution between the two photosystems in higher plants. Biochim Biophys Acta **1777**(5): 425–432

van Oort B, Amunts A, Borst JW, van Hoek A, Nelson N, van Amerongen H, Croce R (2008) Picosecond fluorescence of intact and dissolved PSI-LHCI crystals. Biophys J **95**(12): 5851–5861

Vener AV, van Kan PJ, Rich PR, Ohad I, Andersson B (1997) Plastoquinol at the quinol oxidation site of reduced cytochrome bf mediates signal transduction between light and protein phosphorylation: thylakoid protein kinase deactivation by a single-turnover flash. Proc Natl Acad Sci U S A **94**(4): 1585–1590

Walters RG (2005) Towards an understanding of photosynthetic acclimation. J Exp Bot **56**(411): 435–447

Warren SC, Margineanu A, Alibhai D, Kelly DJ, Talbot C, Alexandrov Y, Munro I, Katan M, Dunsby C, French PMW (2013) Rapid global fitting of large fluorescence lifetime imaging microscopy datasets. Plos One **8**(8):e70687

Wientjes E, Croce R (2012) PMS: photosystem I electron donor or fluorescence quencher. Photosyn Res **111**(1–2): 185–191

Wientjes E, Philippi J, Borst JW, van Amerongen H (2017) Imaging the photosystem I/photosystem II chlorophyll ratio inside the leaf. Biochim Biophys Acta **1858**(3): 259–265

Wientjes E, van Amerongen H, Croce R (2013) Quantum yield of charge separation in photosystem II: functional effect of changes in the antenna size upon light acclimation. J Phys Chem B **117**(38): 11200–11208

Wientjes E, van Stokkum IHM, van Amerongen H, Croce R (2011) The role of the individual lhcas in photosystem I excitation energy trapping. Biophys J **101**(3): 745–754

Wietrzynski W, Schaffer M, Tegunov D, Albert S, Kanazawa A, Plitzko JM, Baumeister W, Engel BD (2020) Charting the native architecture of Chlamydomonas thylakoid membranes with single-molecule precision. Elife **9**: e53740

Wood WHJ, Barnett SFH, Flannery S, Hunter CN, Johnson MP (2019) Dynamic thylakoid stacking is regulated by LHCII phosphorylation but not its interaction with PSI. Plant Physiol **180**(4): 2152–2166

Wood WHJ, MacGregor-Chatwin C, Barnett SFH, Mayneord GE, Huang X, Hobbs JK, Hunter CN, Johnson MP (2018) Dynamic thylakoid stacking regulates the balance between linear and cyclic photosynthetic electron transfer. Nat Plants **4**(2): 116–127

Zhang XJ, Fujita Y, Tokutsu R, Minagawa J, Ye S, Shibata Y (2021) High-speed excitation-spectral microscopy uncovers in situ rearrangement of light-harvesting apparatus in Chlamydomonas during state transitions at submicron precision. Plant Cell Physiol **62**(5): 872–882

Zito F, Finazzi G, Delosme R, Nitschke W, Picot D, Wollman FA (1999) The qo site of cytochrome b(6)f complexes controls the activation of the LHCII kinase. Embo J **18**(11): 2961–2969